Dalton Transactions

RSC Publishing

PAPER

View Article Online
View Journal | View Issue

Cite this: *Dalton Trans.*, 2013, **42**, 12699

Supported monodisperse Pt nanoparticles from $[Pt_3(CO)_3(\mu_2\text{-}CO)_3]_5^{2-}$ clusters for investigating support–Pt interface effect in catalysis†

Guangxu Chen, Huayan Yang, Binghui Wu, Yanping Zheng and Nanfeng Zheng*

Received 9th April 2013,
Accepted 2nd May 2013

DOI: 10.1039/c3dt50942g

www.rsc.org/dalton

Here we present a surfactant-free strategy to prepare supported monodisperse Pt nanoparticles from molecular $[Pt_3(CO)_3(\mu_2\text{-}CO)_3]_5^{2-}$ clusters. The strategy allows facile deposition of same-sized Pt nanoparticles on various oxide supports to unambiguously study the interface effect between noble metal and metal oxide in catalysis. In this study, Fe_2O_3 is demonstrated to be a superior support over TiO_2, CeO_2 and SiO_2 to prepare highly active supported Pt nanoparticles for CO oxidation, which indicates that the interfaces between Pt and iron oxide are the active sites for O_2 activation and CO oxidation.

Introduction

Heterogeneous catalysts with fine metal particles loaded on high-surface-area solids play an important role in industrial chemistry.[1,2] For example, supported Pt-based heterogeneous nanocatalysts have been widely used in hydrogenation,[3,4] oxidative dehydrogenation,[5–7] oxygen reduction reaction (ORR),[8–12] and so on. In general, supported metal nanocatalysts are complex systems with performance determined by a combination of several parameters which at least include the composition, particle size and structure of metal nanoparticles, and also the interfaces between metal and supports.[9,13–17] In order to design and prepare a supported metal nanocatalyst with optimized performance, one needs to deeply understand how the overall performance is influenced by each parameter individually. However, traditional synthetic strategies to prepare supported metal nanocatalysts are based on wet impregnation methods pioneered by Universal Oil Products in the 1940s.[18–20] The methods typically involve the deposition of the high-valent metal precursors on supports followed by thermal or chemical reduction of the deposited precursors to directly yield metal nanoparticles on the supports. Those methods do not allow us to precisely control an individual influencing parameter in a supported metal nanocatalyst. In particular, the interface between metal and supports is difficult to be precisely engineered while keeping other parameters the same. Such a situation prevents us from drawing unambiguous conclusions about the interface effect in heterogeneous catalysis.

In recent years, research efforts have thus been devoted to the colloidal deposition method to better control the parameters of supported metal nanocatalysts.[21–23] In the colloidal deposition method, well-defined metal nanoparticles are prepared and then deposited on supports to better control the composition, size, and shape of the metal nanoparticles. However, in order to obtain high-quality monodisperse nanocrystals, bulky capping agents, such as surfactants,[24] biomaterials,[19,20] polymers[25–29] or fatty ligands,[11,12,30–32] are typically employed in the synthesis. The presence of bulky capping agents on the surface of as-prepared nanoparticles would more or less block the catalytic sites. Pre-treatments are often required to clean their surfaces to make them active for catalysis.[8,12,21,22,33,34] However, one could not guarantee that a change of the uniform nature of the pre-made nanoparticles would not occur during the surface cleaning process, which could make it meaningless to pre-make uniform metal nanoparticles. The development of methods that allow the direct precision synthesis of catalytic nanomaterials is highly desirable.

Dianionic $[Pt_3(CO)_3(\mu_2\text{-}CO)_3]_n^{2-}$ clusters have been reported as unique precursors to prepare carbon-supported monodisperse Pt nanoparticles for electrocatalysis by Higuchi *et al.*[35,36] In this work, we now demonstrate that the $[Pt_3(CO)_3(\mu_2\text{-}CO)_3]_5^{2-}$ clusters can also be used as the precursors for the preparation of surface-clean monodisperse Pt nanoparticles supported on various high-surface-area oxide supports (*i.e.*, TiO_2, CeO_2, Fe_2O_3 and SiO_2) for investigating support–Pt interface effect in catalysis. Without the need of any pre-treatment, the prepared supported catalysts exhibit support-dependent catalytic

State Key Laboratory for Physical Chemistry of Solid Surfaces, Collaborative Innovation Center of Chemistry for Energy Materials, and Department of Chemistry, College of Chemistry and Chemical Engineering, Xiamen University, Xiamen 361005, China. E-mail: nfzheng@xmu.edu.cn; Fax: +86 592 2183047; Tel: +86 592 2186821

†Electronic supplementary information (ESI) available: Experimental details and data. See DOI: 10.1039/c3dt50942g

performance in CO oxidation. Fe_2O_3 is revealed as a superior support over TiO_2, CeO_2 and SiO_2 to fabricate highly active supported Pt nanocatalysts for CO oxidation.

Experimental

Materials

All chemicals were commercially available and used as received without further purification. Chloroplatinic acid ($H_2PtCl_6{\cdot}6H_2O$) was purchased from Sinopharm Chemical Reagent Co. Ltd (Shanghai, China). Cerium dioxide and SiO_2 nanoparticles were purchased from Sigma Aldrich. TiO_2 nanoparticles (P25) and Fe_2O_3 nanoparticles were purchased from Degussa and Alfa Aesar, respectively. CO (99.99%) was obtained from Linde Gas.

Characterizations

A Varian Cary 5000 UV-visible spectrometer was used to record the UV-visible spectra of the reaction solution before and after reaction. The infrared (IR) spectra of the solid samples were recorded from 400 to 4000 cm^{-1} on a Nicolet 380 FTIR spectrometer (Thermo Electron Corporation) by using KBr pellets. IR spectra of the liquid samples were recorded from 900 to 4000 cm^{-1} with the liquid film formed in the middle of two CaF_2 pellets. X-ray photoelectron spectroscopy (XPS) measurements were carried out in a UHV system using a monochromatized Al K_α radiation (1486.6 eV) and an Omicron Sphera II hemispherical electron energy analyser. Binding energies reported herein are with reference to C (1s) at 284.5 eV. The TEM images and high resolution TEM (HRTEM) image were acquired using TECNAI F30 transmission electron microscope, which was operated at 300 kV. The TEM samples were made by placing a 2 μL sample on a carbon coated copper grid and finally dried in the air. Mass spectrum was obtained on an ESQUIRE 3000 plus (Bruker) instrument operating in electrospray ionization and negative mode. The concentrations of CO and CO_2 in the effluent gas were analysed by an on-line gas chromatograph (FULI 9790II, TDX-01 column) using N_2 as the carrier gas. The dispersion of the Pt catalysts was measured by pulse adsorption of CO on a Micromeritics Auto Chem II 2920 chemisorption analyzer at 50 °C.

Preparation of $[Pt_3(CO)_3(\mu_2\text{-}CO)_3]_5^{2-}$ clusters

Aqueous solution of chloroplatinic acid (H_2PtCl_6) (0.1 M, 0.5 mL) mixed with 10 mL dimethylformamide (DMF) was reduced at 50 °C for 12 h in a glass pressure vessel which was charged with 0.1 MPa CO. The yellow reaction solution gradually turned blue-green after reaction. The resulting solution was used for further preparation of supported Pt nanoparticles without any purification or other treatments.

Preparation of different-sized Pt nanoparticles loaded on P25

In a typical experiment, 1 mL DMF solution of $[Pt_3(CO)_3(\mu_2\text{-}CO)_3]_5^{2-}$ clusters prepared above was firstly diluted with 4 mL DMF. The as-prepared DMF solution of $[Pt_3(CO)_3(\mu_2\text{-}CO)_3]_5^{2-}$ clusters was mixed with 60 mg TiO_2 (P25) under vigorous stirring. The as-made composite was then stirred in air at room temperature for 3 h. To control the size of the Pt nanoparticles, different temperatures or ripening time were modified. Pt nanoparticles loaded on P25 with size of 1.8, 2.5 and 2.8 nm were produced by heating the reaction composites at 100 °C for 3 h, 150 °C for 3 h and 150 °C for 9 h, respectively. The final precipitates were centrifuged or filtered, washed with ethanol for several times, dried in vacuum oven and used for catalysis and further characterization.

Preparation of similar-sized Pt nanoparticles loaded on different supports

Pt (2.2 ± 0.2 nm) nanoparticles loaded on P25. 10.5 mL (10 mg Pt) DMF solution of $[Pt_3(CO)_3(\mu_2\text{-}CO)_3]_5^{2-}$ clusters mixed with 250 mg P25 was stirred in the air at room temperature for 12 h to yield P25-supported Pt nanoparticles.

Pt (2.0 ± 0.2 nm) nanoparticles loaded on CeO_2. 10.5 mL (10 mg Pt) DMF solution of $[Pt_3(CO)_3(\mu_2\text{-}CO)_3]_5^{2-}$ clusters mixed with 250 mg CeO_2 was stirred in the air at room temperature for 12 h to yield Pt nanoparticles supported on CeO_2.

Pt (2.0 ± 0.3 nm) nanoparticles loaded on Fe_2O_3. 10.5 mL (10 mg Pt) DMF solution of $[Pt_3(CO)_3(\mu_2\text{-}CO)_3]_5^{2-}$ clusters mixed with 500 mg Fe_2O_3 was stirred and heated at 150 °C for 3 h to give Fe_2O_3-supported Pt nanoparticles.

Pt (2.0 ± 0.3 nm) nanoparticles loaded on SiO_2. Before the deposition of Pt nanoparticles, the surface of SiO_2 was modified with $-NH_2$ by mixing 1.0 g SiO_2 and 100 μL (3-aminopropyl)trimethoxysilane in 100 mL toluene at 50 °C overnight. The product was separated *via* centrifugation, washed with ethanol for several times and dried in vacuum. 10.5 mL DMF solution of $[Pt_3(CO)_3(\mu_2\text{-}CO)_3]_5^{2-}$ clusters (10 mg Pt) mixed with 220 mg surface-modified SiO_2 was stirred and heated at 150 °C for 3 h to give the SiO_2 supported Pt nanoparticles.

Preparation of Pt nanoparticles loaded on different supports with conventional impregnation method

Pt nanoparticles loaded on SiO_2. An aqueous solution of chloroplatinic acid (H_2PtCl_6) (0.1 M, 0.25 mL) and 200 mg $-NH_2$ modified SiO_2 were mixed with 10 mL water and then stirred at room temperature. The precipitate was separated *via* centrifugation. Before reducing under H_2 atmosphere at 200 °C for 2 h, the precipitate was first dried in the vacuum oven for 12 h.

Pt nanoparticles loaded on P25. An aqueous solution of chloroplatinic acid (H_2PtCl_6) (0.1 M, 0.25 mL), 200 mg P25 and 0.1 mL ammonia (28%) were mixed with 10 mL water and then stirred at room temperature. The precipitate was separated *via* centrifugation. Before reducing under H_2 atmosphere at 200 °C for 2 h, the precipitate was first dried in the vacuum oven for 12 h.

Catalysis of CO oxidation

The catalysis of CO oxidation was carried out in a continuous flow fix-bed glass reactor with an inner diameter of 5 mm. CO conversion was detected by an on-line gas chromatography.

The gas mixture of air (40 mL min^{-1}) and CO (10 mL min^{-1}, 5 vol% in N_2) was controlled by mass flow controllers at atmospheric pressure and passed through the catalysts at a space velocity of 270 L h^{-1} g^{-1}_{Pt}. The reactor was heated by an electrical heater controlled by a temperature controller. The temperature of the reactor was incrementally raised from room temperature to 170 °C. The gas after catalysis reaction was sampled every ten degree by an auto-sampler.

CO conversion (X_{CO}) is calculated as:

$$X_{CO}\ \text{conversion}\ (\%) = \frac{[CO]_{in} - [CO]_{out}}{[CO]_{in}} \times 100$$

The TOF (turnover frequencies) were calculated based on the specific rate and the dispersion of Pt. Specific reaction rates and TOF of Pt-based catalysts at different temperatures were obtained by decreasing the weight of catalyst to ensure the CO conversion below 35%. The TOF were calculated as:

$$\text{TOF} = \frac{X_{CO} \times [CO]_{in} \times V}{N_{\text{active sites}}}\ \text{in}\ [\text{molecules Pt}_{\text{sites}}{}^{-1}\ \text{s}^{-1}]$$

V is the total mole flow rate. Based on Arrhenius equation, E_a and A were determined:

$$k = Ae^{-(E_a/RT)}$$

$$\ln k = \ln A - \frac{E_a}{RT}$$

where k is the rate constant of a chemical reaction at an absolute temperature T (in Kelvin), A is the pre-exponential factor, E_a is the apparent activation energy, and R is the standard gas constant. In our case, TOF were used as the rate constant in the Arrhenius' equation. The slopes of ln(TOF) *versus* T^{-1} plots were used to determine E_a.

Results and discussion

$[Pt_3(CO)_3(\mu_2\text{-}CO)_3]_5^{2-}$ clusters

To prepare the $[Pt_3(CO)_3(\mu_2\text{-}CO)_3]_5^{2-}$ clusters, H_2PtCl_6 was reacted with CO in DMF without any surfactants or polymers at 50 °C for 12 h in a glass pressure vessel which was charged with 0.1 MPa CO. At the end of the reaction, the color of the solution changed from yellow to blue-green (Fig. 1a), indicating the formation of platinum carbonyl clusters. It has been well documented that the reaction of H_2PtCl_6 with CO often leads to the formation of $[Pt_3(CO)_3(\mu_2\text{-}CO)_3]_n^{2-}$ clusters.[37–40] With a columnar structure, the $[Pt_3(CO)_3(\mu_2\text{-}CO)_3]_n^{2-}$ clusters can be considered as stacking oligomers of common planar triplatinum hexacarbonyl components along the pseudo-threefold axis through Pt–Pt bonding.[38] The $[Pt_3(CO)_3(\mu_2\text{-}CO)_3]_n^{2-}$ clusters with different number (n) of planar triplatinum hexacarbonyl units exhibit different absorption bands, which have been studied by experiments and theoretical calculations.[37–40]

To determine the degree of polymerization of the as-made clusters, UV-vis spectra were recorded for the DMF solution of

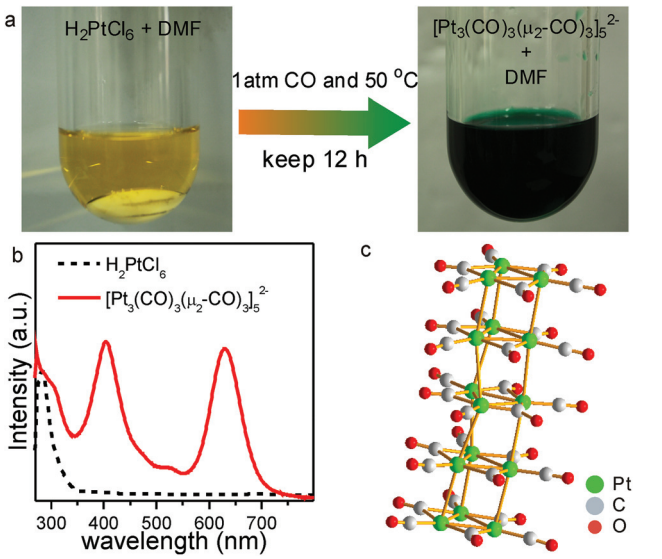

Fig. 1 (a) Photographs and (b) UV-vis spectra of DMF solutions before and after reaction. (c) The structure of the $[Pt_3(CO)_3(\mu_2\text{-}CO)_3]_5^{2-}$ cluster.

H_2PtCl_6 before and after reaction (Fig. 1b). Compared with the H_2PtCl_6 solution, two new peaks at 400 nm and 630 nm appear for the clusters in DMF, consistent with that of the $[Pt_3(CO)_3(\mu_2\text{-}CO)_3]_5^{2-}$.[39,40] The model of the $[Pt_3(CO)_3(\mu_2\text{-}CO)_3]_5^{2-}$ cluster is presented in Fig. 1c. Only the two characteristic peaks appear in the spectrum indicates that only one kind of cluster, $[Pt_3(CO)_3(\mu_2\text{-}CO)_3]_5^{2-}$, formed in the solution. The polymerization of the cluster was confirmed by our electrospray ionization mass spectrometry (ESI-MS) measurements. The cluster displays a well-resolved peak at 1883.2 m/z under negative ion mode (Fig. 2a), matching well with that of the calculated one for the $[Pt_3(CO)_3(\mu_2\text{-}CO)_3]_5^{2-}$ dianionic cluster. The infrared (IR) spectrum of the DMF solution after reaction also clearly revealed two carbonyl absorption bands at 2050 and 1960 cm^{-1} (Fig. 2b), which are ascribed to the terminal and edge-bridging carbonyl groups, respectively.[41]

Pt nanoparticles with different sizes

As the Pt atoms in the clusters are in negative oxidation state, the size of the clusters can be adjusted towards higher degree of polymerization by spontaneous air oxidation.[39] Once the two electrons on each cluster were lost, the preparation of monodisperse Pt nanoparticles from the clusters would be possible. When the DMF solution of $[Pt_3(CO)_3(\mu_2\text{-}CO)_3]_5^{2-}$ clusters were simply exposed to air for 2 days, uniform Pt nanoparticles were produced but heavily aggregated (Fig. S1†) because of the high surface energy of the fine nanoparticles. Inspired by our previous work where the aggregation of Pt nanoparticles can be prevented by introducing supports during their synthesis,[42] we thus dispersed high-surface-area titanium oxide (P25) in the DMF solution before exposing the $[Pt_3(CO)_3(\mu_2\text{-}CO)_3]_5^{2-}$ clusters to air. After exposure to air for several hours followed by thermal ripening in the DMF solution, the as-made product was separated *via* centrifugation and characterized

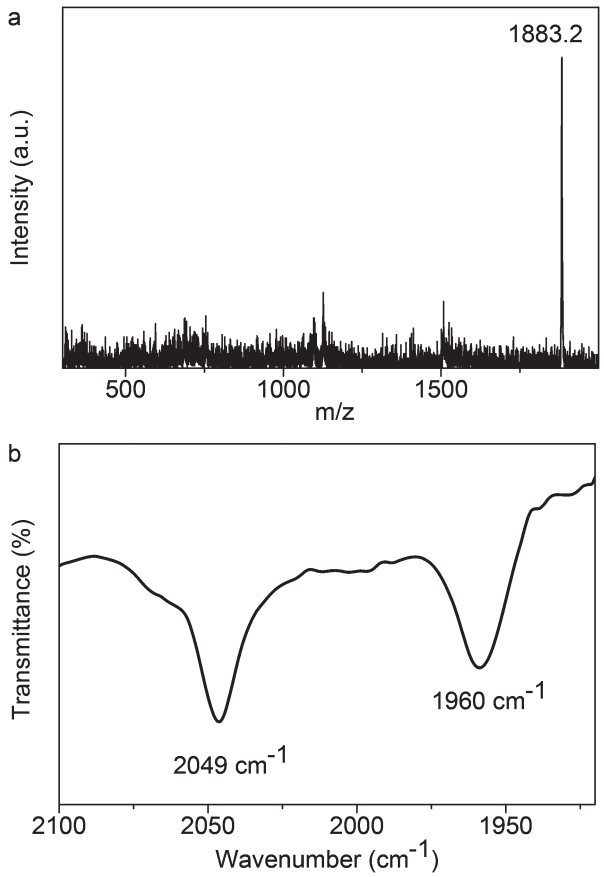

Fig. 2 (a) ESI-MS spectrum of $[Pt_3(CO)_3(\mu_2\text{-}CO)_3]_5^{2-}$ clusters under negative mode. (b) The infrared spectrum of $[Pt_3(CO)_3(\mu_2\text{-}CO)_3]_5^{2-}$ clusters in DMF solution.

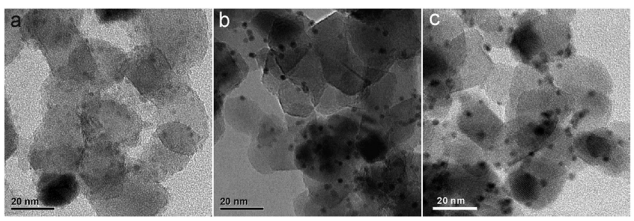

Fig. 3 The representative TEM images of Pt nanoparticles with different sizes loaded on P25: (a) 1.8 nm, (b) 2.5 nm, and (c) 2.8 nm.

by TEM. The TEM images (Fig. 3) clearly reveal that supported monodisperse Pt nanoparticles were successfully produced. The single-crystalline nature of the Pt nanoparticles was also confirmed by HRTEM (Fig. S2†). Starting from $[Pt_3(CO)_3(\mu_2\text{-}CO)_3]_5^{2-}$ cluster precursors, we found in this work that the size of Pt nanoparticles can be further tuned by controlling the oxidation process. By tuning the thermal ripening time, P25-supported Pt nanoparticles with sizes varied from 1.8 nm to 2.8 nm were obtained (Fig. 3a–c).

After being separated from solution, the as-prepared P25-supported Pt nanoparticles were subjected to IR spectral analysis. In contrast with $[Pt_3(CO)_3(\mu_2\text{-}CO)_3]_5^{2-}$ clusters, no carbonyl absorption bands at 2050 and 1960 cm^{-1} were observed for

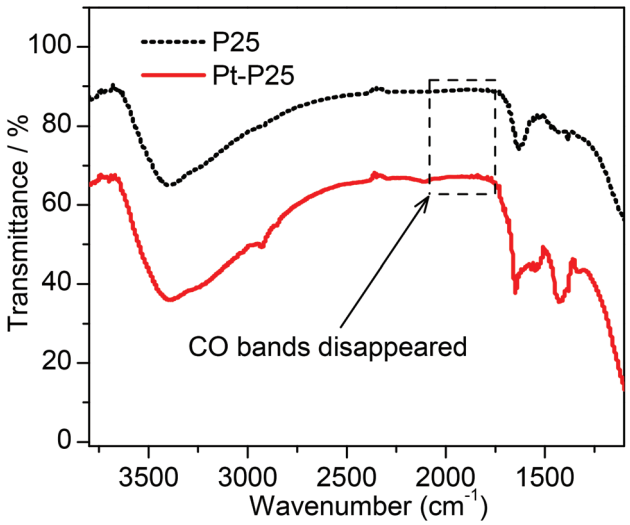

Fig. 4 The infrared spectrum of Pt–P25 after exposure in the air.

P25-supported Pt nanoparticles (Fig. 4), indicating that CO molecules were dissociated from the cluster precursors during the oxidation and ripening process. The obtained supported Pt nanoparticles thus possess clean exposure surfaces, making them promising candidate for catalysis.

Pt nanoparticles loaded on different supports

Starting from $[Pt_3(CO)_3(\mu_2\text{-}CO)_3]_5^{2-}$ clusters which can be easily obtained *in situ* by reducing H_2PtCl_6 by CO in DMF, supported surface-clean uniform Pt nanoparticles are readily prepared by simple mixing and ripening processes. Such a feature has motivated us to apply the synthetic strategy to systematically prepare a series of supported Pt nanoparticles to address some fundamental aspects in designing Pt nanocatalysts with optimized catalytic performances. For example, the interface effect in heterogeneous catalyst usually plays a crucial role in the catalytic activity. In many cases, however, the interface effect is coupled with the influence from other factors such as the size of the metal nanoparticles. Therefore, to clearly address which interface between noble metal and metal oxide is better than others, one should prepare the same-sized metal nanoparticles deposited on various supports for comparison studies.

To study the interface effect between Pt and metal oxide of supported Pt nanocatalysts, we have attempted to employ $[Pt_3(CO)_3(\mu_2\text{-}CO)_3]_5^{2-}$ as the precursor to prepare supported uniform Pt nanoparticles on various supports (*i.e.*, P25, CeO_2, Fe_2O_3 and SiO_2). The same amount of $[Pt_3(CO)_3(\mu_2\text{-}CO)_3]_5^{2-}$ clusters were mixed with supports and subjected to air oxidation to form similar-sized Pt nanoparticles on the supports. The representative TEM images (Fig. 5) reveal that the obtained Pt nanoparticles are of similar size (~2 nm) and are well dispersed on the supports. In order to have Pt nanoparticles also deposited on SiO_2, it should be noted that the surface of SiO_2 was pre-modified with $-NH_2$ by hydrolyzing (3-aminopropyl)trimethoxysilane at 50 °C overnight in toluene solution. Because of the weak interaction between $[Pt_3(CO)_3(\mu_2\text{-}CO)_3]_5^{2-}$

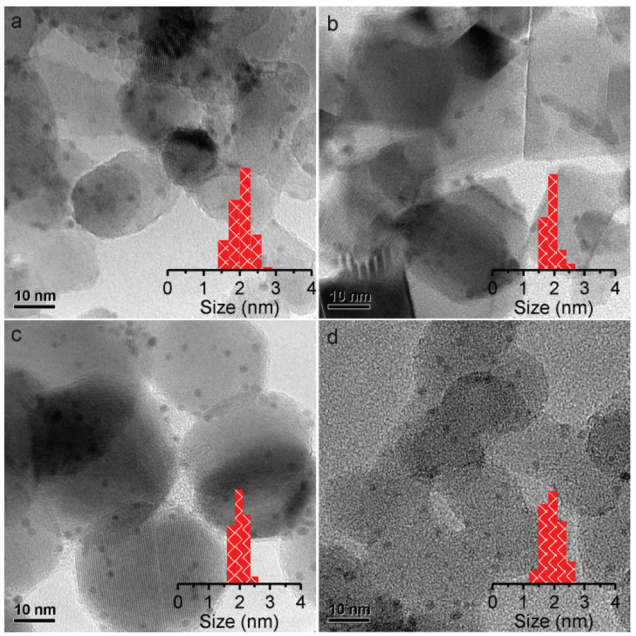

Fig. 5 The representative TEM images of Pt nanoparticles loaded on different supports: (a) P25, (b) CeO_2, (c) Fe_2O_3, and (d) SiO_2. The histograms show the size distribution of the Pt nanoparticles loaded on different supports, respectively.

clusters and the unmodified SiO_2 surface, without the $-NH_2$ modification the Pt nanoparticles would aggregate on SiO_2 (Fig. S3†). The sizes of the Pt nanoparticles supported on P25, CeO_2, Fe_2O_3 and SiO_2 (denoted as Pt–TiO_2, Pt–CeO_2, Pt–Fe_2O_3 and Pt–SiO_2) are 2.2 ± 0.2 nm, 2.0 ± 0.2 nm, 2.0 ± 0.3 nm and 2.0 ± 0.3 nm, respectively. For comparison, Pt nanoparticles loaded on different supports were prepared with a conventional impregnation method.[43–45] The as-prepared SiO_2- and P25-supported Pt nanoparticles are rather polydispersed in size (Fig. S4†). What is worse, the Pt precursor cannot be absorbed on the 50 nm Fe_2O_3 nanoparticles under acidic condition or in aqueous solutions of high pH-value (10–11). The difficulty for the conventional impregnation method to prepare monodisperse Pt nanoparticles highlights the advantages of our strategy. With a similar size distribution of Pt nanoparticles, these supported Pt nanocatalysts are an ideal system to study the interface effect in catalysis.

Interface effect in catalysis

CO oxidation was chosen as the probe reaction to investigate the interface effect. As clearly illustrated in Fig. 6a, the four supported catalysts exhibit quite different activities in CO oxidation. The Pt–Fe_2O_3 catalyst displayed the best catalytic performance with complete conversion of CO at near room temperature (Fig. 6a). The catalyst also displayed a stable activity in the entire range of temperatures studied (30 to 160 °C). No decrease in the activity was observed during either heating or cooling process. In comparison, all the other catalysts (*i.e.*, Pt–TiO_2, Pt–CeO_2, Pt–SiO_2) achieved complete CO conversion only above 70 °C, higher than that by Pt–Fe_2O_3.

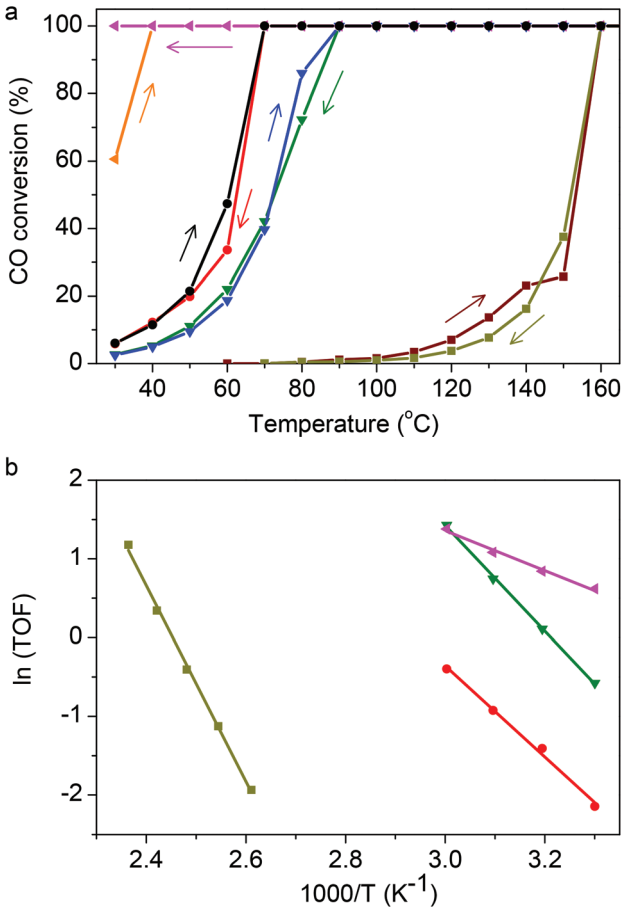

Fig. 6 (a) Heating and cooling (10 °C min^{-1}) light-off curves of CO conversion against the temperature for the four studied catalysts. (b) Kinetic rate data for CO oxidation on four studied catalysts: (●) Pt–P25, (▼) Pt–CeO_2, (◀) Pt–Fe_2O_3, and (■) Pt–SiO_2.

The enhanced activity of the Pt–Fe_2O_3 catalyst could be explained by the strong metal support interaction between Pt nanoparticles and iron oxide. FeO_x is commonly recognized as the active phase for oxygen activation for CO oxidation.[46–50] Combined with Pt nanoparticles which serve as the absorption sites for CO, the synergetic effect of the interface between FeO_x and Pt promotes the reaction of CO oxidation.[45,51] Guided by these insights, we prepared the catalyst of unsupported Pt nanoparticles mixing with iron oxide (physical mixing). The performance of the catalyst was also investigated for the catalysis of CO oxidation under the same condition. As illustrated in Fig. S5,† the catalyst exhibited a poor activity for CO oxidation, indicating that the physical mixing strategy for the preparation of the catalyst reduced the interfaces between Pt and iron oxide and lead to the decrease of activity, which further confirmed the importance of the interfaces. The interface effect is not optimal in Pt–TiO_2 and Pt–CeO_2 catalysts and even worse in the case of an inert support such as SiO_2. As illustrated in Fig. 6a, the complete conversion of CO for Pt–SiO_2 catalyst was only achieved above 160 °C. The catalysts after catalysis were also characterized by TEM (Fig. S6†). The results indicate that the catalysts displayed high thermal stability except for

Pt–SiO_2. The size of Pt nanoparticles loaded on SiO_2 increased from 2.0 nm to 2.5 nm, indicating that the interaction between Pt and SiO_2 was weak. But it should be noted that the Pt nanoparticles loaded on SiO_2 exhibited strong adsorption ability for CO in our CO titration experiments that were used to determine the metal dispersions and TOFs (Fig. S7†). These results imply that a synergetic effect occurred at the interfaces between Pt nanoparticles and Fe_2O_3, P25 and CeO_2 supports, but was not present in the Pt–SiO_2 catalyst. This phenomenon has been denoted as the 'support effect' in surface science and catalysis.

To provide deep insight into the kinetic and energetics of CO oxidation in the presence of different catalysts, turnover frequencies (TOF) at different temperatures before the complete conversion of CO were calculated for the different Pt-based catalysts (Fig. S8†). As shown in the Arrhenius plots (Fig. 6b), the reaction rates on Pt–Fe_2O_3 at 30 °C were about 3 and 16 times higher than those on Pt–CeO_2 and Pt–P25 under the same conditions, respectively. The apparent activation energies of Pt–Fe_2O_3, Pt–P25, Pt–CeO_2, and Pt–SiO_2 catalysts are 21.1 ± 1.4 kJ mol^{-1}, 48.14 ± 2.5 kJ mol^{-1}, 55.8 ± 1.1 kJ mol^{-1} and 103.6 ± 2.5 kJ mol^{-1}, respectively. The different apparent activation energies clearly indicate that the nature of their active sites is significantly different among the four catalysts. These results demonstrate that the metal-support interaction could change the reaction pathway. With the lowest energy barrier among the four studied catalysts, the Pt–Fe_2O_3 catalyst would be a promising catalytic system for CO removal at low temperature. Time-on-stream experiments under dry and moist atmospheres were carried out on the oxidation of CO over the Pt–Fe_2O_3 catalyst at 30 °C. As demonstrated in Fig. 7, the activity of the Pt–Fe_2O_3 catalyst under dry atmosphere decreased quickly from 100% conversion to 50% in 400 min. In comparison, under the humid atmosphere (50 ± 5%), the Pt–Fe_2O_3 catalyst can realize full conversion of CO at 30 °C without any decrease of the activity in 2500 min, which indicates that the stability of the catalysts were enhanced by water. However, it should be noted that no obvious change in the morphology of the Pt nanoparticles was observed by TEM for the catalyst after catalysis in dry or humid conditions (Fig. S9†). Further study of the surface properties of the Pt nanoparticles loaded on different supports was carried out with X-ray photoelectron spectroscopy (XPS). As revealed in Fig. S10,† the Pt $4f_{7/2}$ peaks of Pt–P25, Pt–CeO_2 and Pt–Fe_2O_3 are located at 71.2 eV, 71.1 eV and 71.1 eV, respectively, which are consistent with metallic Pt. A molecule-level understanding of the relationship between the Pt–FeO_x interfaces and the enhanced catalysis is still needed.

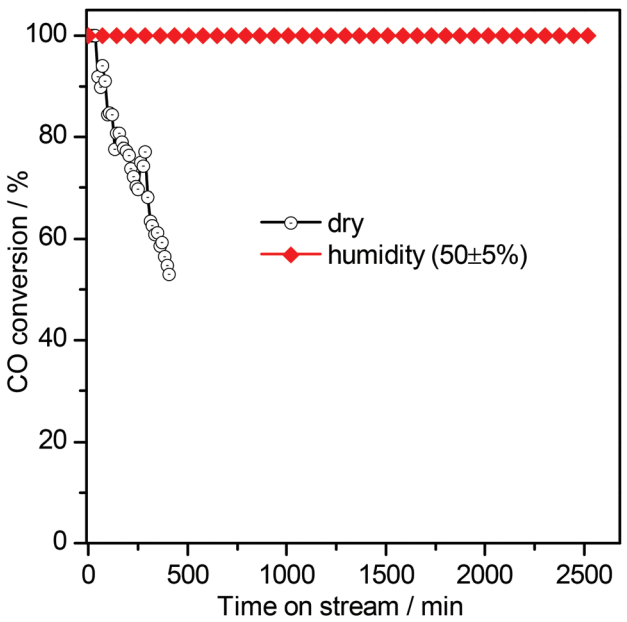

Fig. 7 (a) Effects of moisture and durability on the oxidation of CO over Pt–Fe_2O_3 catalysts at 30 °C.

Conclusion

In conclusion, we demonstrate a simple and effective strategy to prepare supported surface-clean Pt nanoparticles from di-anionic $[Pt_3(CO)_3(\mu_2\text{-}CO)_3]_5^{2-}$ clusters. Supported monodisperse Pt nanoparticles are readily prepared by simply mixing the clusters with desired supports in air. While the size of the Pt nanoparticles can be varied by the thermal ripening process, it is possible to prepare supported Pt nanoparticles with a similar size but loaded on different supports (*i.e.*, TiO_2, CeO_2, Fe_2O_3, and SiO_2). The obtained catalysts were applied to investigate the interface effect of oxide-supported Pt nanoparticles in CO oxidation. Fe_2O_3 was demonstrated to be a superior support over TiO_2, CeO_2 and SiO_2 to prepare highly active supported Pt nanoparticles for CO oxidation. The complete CO oxidation at room temperature was readily achieved by the as-obtained Pt–Fe_2O_3 catalyst.

Acknowledgements

We thank the MOST of China (2011CB932403), the NSFC (21131005, 21021061, 20925103, 20923004), and the Fok Ying Tung Education Foundation (121011) for the financial support.

Notes and references

1 D. Astruc, F. Lu and J. R. Aranzaes, *Angew. Chem., Int. Ed.*, 2005, **44**, 7852–7872.
2 M. Stratakis and H. Garcia, *Chem. Rev.*, 2012, **112**, 4469–4506.
3 C. W. Chen, T. Serizawa and M. Akashi, *Chem. Mater.*, 1999, **11**, 1381–1389.
4 K. M. Bratlie, H. Lee, K. Komvopoulos, P. D. Yang and G. A. Somorjai, *Nano Lett.*, 2007, **7**, 3097–3101.
5 S. Vajda, M. J. Pellin, J. P. Greeley, C. L. Marshall, L. A. Curtiss, G. A. Ballentine, J. W. Elam, S. Catillon-

Mucherie, P. C. Redfern and F. Mehmood, *Nat. Mater.*, 2009, **8**, 213–216.
6 C. Keresszegi, T. Mallat, J. D. Grunwaldt and A. Baiker, *J. Catal.*, 2004, **225**, 138–146.
7 D. H. Parker, C. L. Pettiette-Hall, Y. Li, R. T. McIver Jr. and J. C. Hemminger, *J. Phys. Chem.*, 1992, **96**, 1888–1894.
8 J. B. Wu, J. L. Zhang, Z. M. Peng, S. C. Yang, F. T. Wagner and H. Yang, *J. Am. Chem. Soc.*, 2010, **132**, 4984–4985.
9 V. R. Stamenkovic, B. Fowler, B. S. Mun, G. Wang, P. N. Ross, C. A. Lucas and N. M. Markovic, *Science*, 2007, **315**, 493–497.
10 W. Yang, X. L. Wang, F. Yang, C. Yang and X. R. Yang, *Adv. Mater.*, 2008, **20**, 2579–2587.
11 C. Wang, H. Daimon, Y. Lee, J. Kim and S. H. Sun, *J. Am. Chem. Soc.*, 2007, **129**, 6974–6975.
12 C. Wang, H. Daimon, T. Onodera, T. Koda and S. Sun, *Angew. Chem., Int. Ed.*, 2008, **47**, 3588–3591.
13 M. Arenz, K. J. J. Mayrhofer, V. Stamenkovic, B. B. Blizanac, T. Tomoyuki, P. N. Ross and N. M. Markovic, *J. Am. Chem. Soc.*, 2005, **127**, 6819–6829.
14 X. Q. Huang, Z. P. Zhao, J. M. Fan, Y. M. Tan and N. F. Zheng, *J. Am. Chem. Soc.*, 2011, **133**, 4718–4721.
15 N. Tian, Z. Y. Zhou, S. G. Sun, Y. Ding and Z. L. Wang, *Science*, 2007, **316**, 732–735.
16 S. J. Tauster, S. C. Fung, R. T. K. Baker and J. A. Horsley, *Science*, 1981, **211**, 1121–1125.
17 S. J. Tauster, *Acc. Chem. Res.*, 1987, **20**, 389–394.
18 J. Yang, V. Tschamber, D. Habermacher, F. Garin and P. Gilot, *Appl. Catal., B*, 2008, **83**, 229–239.
19 G. A. Somorjai and J. Y. Park, *Angew. Chem., Int. Ed.*, 2008, **47**, 9212–9228.
20 M. Haruta, *CATTECH*, 2002, **6**, 102–115.
21 N. Zheng and G. D. Stucky, *J. Am. Chem. Soc.*, 2006, **128**, 14278–14280.
22 M. Comotti, W. C. Li, B. Spliethoff and F. Schuth, *J. Am. Chem. Soc.*, 2006, **128**, 917–924.
23 H. F. Yin, C. Wang, H. G. Zhu, S. H. Overbury, S. H. Sun and S. Dai, *Chem. Commun.*, 2008, 4357–4359.
24 H. Lee, S. E. Habas, S. Kweskin, D. Butcher, G. A. Somorjai and P. D. Yang, *Angew. Chem., Int. Ed.*, 2006, **45**, 7824–7828.
25 T. S. Ahmadi, Z. L. Wang, T. C. Green, A. Henglein and M. A. El-Sayed, *Science*, 1996, **272**, 1924–1926.
26 C. K. Tsung, J. N. Kuhn, W. Huang, C. Aliaga, L. I. Hung, G. A. Somorjai and P. D. Yang, *J. Am. Chem. Soc.*, 2009, **131**, 5816–5822.
27 T. S. Ahmadi, Z. L. Wang, A. Henglein and M. A. El-Sayed, *Chem. Mater.*, 1996, **8**, 1161–1163.
28 R. Narayanan and M. A. El-Sayed, *Nano Lett.*, 2004, **4**, 1343–1348.
29 H. Song, F. Kim, S. Connor, G. A. Somorjai and P. D. Yang, *J. Phys. Chem. B*, 2004, **109**, 188–193.
30 S. I. Lim, I. Ojea-Jimenez, M. Varon, E. Casals, J. Arbiol and V. Puntes, *Nano Lett.*, 2010, **10**, 964–973.
31 J. Zhang and J. Y. Fang, *J. Am. Chem. Soc.*, 2009, **131**, 18543–18547.
32 J. Ren and R. D. Tilley, *J. Am. Chem. Soc.*, 2007, **129**, 3287–3291.
33 C. Aliaga, J. Y. Park, Y. Yamada, H. S. Lee, C. K. Tsung, P. D. Yang and G. A. Somorjai, *J. Phys. Chem. C*, 2009, **113**, 6150–6155.
34 J. Zhang, H. Z. Yang, J. Y. Fang and S. Z. Zou, *Nano Lett.*, 2010, **10**, 638–644.
35 E. Higuchi, K. Adachi, S. Nohara and H. Inoue, *Res. Chem. Intermed.*, 2009, **35**, 985–995.
36 E. Higuchi, A. Taguchi, K. Hayashi and H. Inoue, *J. Electroanal. Chem.*, 2011, **663**, 84–89.
37 C. Femoni, M. C. Iapalucci, F. Kaswalder, G. Longoni and S. Zacchini, *Coord. Chem. Rev.*, 2006, **250**, 1580–1604.
38 R. G. Woolley, *Chem. Phys. Lett.*, 1988, **143**, 145–152.
39 B. Le Gratiet, H. Remita, G. Picq and M. O. Delcourt, *Radiat. Phys. Chem.*, 1996, **47**, 263–268.
40 M. Treguer, H. Remita, P. Pernot, J. Khatouri and J. Belloni, *J. Phys. Chem. A*, 2001, **105**, 6102–6108.
41 C. Femoni, F. Kaswalder, M. C. Iapalucci, G. Longoni, M. Mehlstaubl, S. Zacchini and A. Ceriotti, *Angew. Chem., Int. Ed.*, 2006, **45**, 2060–2062.
42 G. X. Chen, Y. M. Tan, B. H. Wu, G. Fu and N. F. Zheng, *Chem. Commun.*, 2012, **48**, 2758–2760.
43 S. Lu, W. W. Lonergan, J. P. Bosco, S. Wang, Y. Zhu, Y. Xie and J. G. Chen, *J. Catal.*, 2008, **259**, 260–268.
44 S. Lu, W. W. Lonergan, Y. Zhu, Y. Xie and J. G. Chen, *Appl. Catal., B*, 2009, **91**, 610–618.
45 Q. Fu, W. X. Li, Y. Yao, H. Y. Liu, H. Y. Su, D. Ma, X. K. Gu and X. H. Bao, *Science*, 2010, **875**, 26–29.
46 M. Shou, H. Takekawa, D. Y. Ju, T. Hagiwara, D. L. Lu and K. I. Tanaka, *Catal. Lett.*, 2006, **108**, 119–124.
47 K. I. Tanaka, Y. Moro Oka, K. Ishigure, T. Yajima, Y. Okabe, Y. Kato, H. Hamano, S. I. Sekiya, H. Tanaka, Y. Matsumoto, H. Koinuma, H. He, C. Zhang and Q. Feng, *Catal. Lett.*, 2004, **92**, 115–121.
48 M. Shou and K. I. Tanaka, *Catal. Lett.*, 2006, **111**, 115–118.
49 K. I. Tanaka, M. Shou, H. He and X. Shi, *Catal. Lett.*, 2006, **110**, 185–190.
50 K. I. Tanaka, H. He, M. Shou and X. Y. Shi, *Catal. Today*, 2011, **175**, 467–470.
51 L. R. Merte, J. Knudsen, F. M. Eichhorn, S. Porsgaard, H. Zeuthen, L. C. Grabow, E. Laegsgaard, H. Bluhm, M. Salmeron, M. Mavrikakis and F. Besenbacher, *J. Am. Chem. Soc.*, 2011, **133**, 10692–10695.